

## Article

# Verification of Tilt Effect on the Performance and Wake of a Vertical Axis Wind Turbine by Lifting Line Theory Simulation

Hidetaka Senga<sup>1,\*</sup>, Hiroki Umemoto<sup>1</sup> and Hiromichi Akimoto<sup>2</sup> 

<sup>1</sup> Department of Naval Architecture and Ocean Engineering, Graduate School of Engineering, Osaka University, Suita 565-0871, Japan

<sup>2</sup> Albatross Technology Inc., Chuo-ku, Tokyo 103-0013, Japan

\* Correspondence: senga@naoe.eng.osaka-u.ac.jp; Tel.: +81-668-797-574

**Abstract:** Renewable energy has received a lot of attention. In recent years, offshore wind power has received particular attention among renewable energies. Fixed-type offshore wind turbines are now the most popular. However, because of the deep seas surrounding Japan, floating types are more preferable. The floating system is one of the factors that raises the cost of floating wind turbines. Vertical axis wind turbines (VAWT) have a low center of gravity and can tilt their rotors. As a result, a smaller floating body and a lower cost are expected. A mechanism called a floating axis wind turbine (FAWT) is expected to further reduce the cost. FAWT actively employs the features of VAWT in order to specialize itself in the area of offshore floating-type wind turbines. The lifting line theory simulation was used in this study to discuss the performance of the FAWT under the tilted conditions and its wake field. The results show that a tilted VAWT recovers faster than an upright VAWT. This suggests that FAWTs can be deployed in high density and efficiently generate energy as an offshore wind farm using VAWTs.



**Citation:** Senga, H.; Umemoto, H.; Akimoto, H. Verification of Tilt Effect on the Performance and Wake of a Vertical Axis Wind Turbine by Lifting Line Theory Simulation. *Energies* **2022**, *15*, 6939. <https://doi.org/10.3390/en15196939>

Academic Editors:  
Francesco Castellani and  
Davide Astolfi

Received: 29 July 2022

Accepted: 16 September 2022

Published: 22 September 2022

**Publisher's Note:** MDPI stays neutral with regard to jurisdictional claims in published maps and institutional affiliations.



**Copyright:** © 2022 by the authors. Licensee MDPI, Basel, Switzerland. This article is an open access article distributed under the terms and conditions of the Creative Commons Attribution (CC BY) license (<https://creativecommons.org/licenses/by/4.0/>).

**Keywords:** vertical axis wind turbine; floating axis wind turbine; lifting line theory; tilt of rotor; wake

## 1. Introduction

In order to achieve the Sustainable Development Goals, various renewable energies have become an active area of research. Offshore wind power's technical potential to meet domestic electricity demands indicates that there is a significant amount of unutilized wind energy [1]. Furthermore, 80% of the world's offshore wind resource potential is located in waters deeper than 60 m [2].

Wind turbines are classified into two types. The first is the horizontal axis wind turbine (HAWT), and the second is the vertical axis wind turbine (VAWT). Each axis type has strong and weak points that arise from structural features, and they are often compared in terms of the power coefficient ( $C_p$ ) [3,4]. The  $C_p$  of VAWT is commonly thought to be lower than that of HAWT, but this is mainly for small wind turbines. In fact, the maximum  $C_p$  of the SANDIA 34 m "Test Bed" Darrieus VAWT showed a maximum  $C_p$  of 0.41 to 0.42 [5,6]. On the other hand, many studies have been conducted to improve the performance of VAWTs. Daegyoun et al. [7] studied the effect of an upstream deflector plate on the power output. Even though the specific model of wind turbine of high solidity was used for their study, the deflector system could increase the local wind velocity around the turbine by tailoring free-stream flow and the power output was proportional to the cube of the wind velocity. A wind lens with several types of diffuser was experimentally studied by Watanabe et al. [8]. They concluded that a wind lens with a Venturi shape, curved diffuser, and shorter flanges was most effective in producing a greater power augmentation. The shapes of arms or strut also have an effect on the performance of the turbines. Hara et al. [9] numerically investigated the effects of arms with different cross sections, such as an NACA0018 airfoil, rectangular and circular, on the power loss of a small VAWT. They decomposed the tangential forces

and resistance torques induced by the arms into pressure- and friction-based components. Their results show that, apart from the manufacturing cost and structural strength, the airfoil cross section is ideal for the arm cross section's shape. Aihara et al. [10] compared several numerical methods to investigate whether these methods could reproduce the strut effect on the performance of a VAWT. Their target was 12 kW H-rotor VAWT and the blade force was simulated using the RANS model, the ALM, and the vortex model. Their results show that the strut influence was significant, especially at a high tip speed ratio, and the RANS model was able to simulate the large influence of the strut better than the other two methods. The effect of the blade's cross-sectional shape was investigated by Hou et al. [11]. They numerically investigated the performance of NACA0012, modified NACA0012, and fish skeleton airfoils. The modified NACA0012 airfoils have cambers which are 3, 5, and 7% of the chord length. The fish skeleton airfoil is passively deformed by the pressure from the fluid and it has a higher lift and lower drag coefficient compared to the NACA0012 airfoil. The blade pitch angle is important for not only HAWTs but also VAWTs. Yang et al. [12] studied, experimentally and numerically, the effect of blade pitch angle on aerodynamic characteristics. Their target was a straight-bladed VAWT with two blades. They obtained an optimum blade pitch angle where the power coefficient of their targeted turbine was the largest. However, they concluded that the blade pitch angle for VAWTs had no significant effect on the power coefficient compared to HAWTs. Because the attack angle of VAWTs' blades continuously varies during one rotor rotation, the effect of active pitch angle control on the power coefficient was investigated numerically by Horb et al. [13]. Their optimized pitch laws could increase the power coefficient by more than 15% in maximum power point tracking mode. Mohammed et al. [14] found that a fixed pitch of  $-2.5$  [deg] could enhance performance of a small-scale straight-bladed Darrieus-type VAWT, although its starting torque capacity could not be improved. Their variable pitch angle of sinusoidal nature could improve the power coefficient despite the low starting capacity.

However,  $C_p$  is one of the factors to consider when comparing wind turbine systems, with power generation cost being the most important. If a wind turbine's construction and maintenance are expensive, the power generation cost is high even if a high-efficiency  $C_p$  turbine is adapted for the system.

Akimoto et al. proposed a floating offshore wind turbine (FOWT) concept, called the floating axis wind turbine (FAWT), that uses a VAWT to reduce power generation cost [15]. There are several types of FOWT that use vertical axis wind turbines, including semi-submersible [16,17] and spar [18,19]. In Akimoto's concept, the latter was adapted to actively utilize the features of VAWTs, such as the low center of gravity and the fact that the power coefficient of VAWTs is difficult to decrease compared to that of HAWTs if the turbine tilts. A straight-blade VAWT is attached to a spar and they rotate together. Power take-off units are installed on the spar above the water's surface, and the unit is moored so as to keep the position of the FAWT and absorb the reaction torque resulting from power generation. The smaller spar is all that is required for FAWTs because it assumes rotor axis tilt, which reduces construction costs. As a result, it is critical to assess VAWT performance under tilted conditions. Figure 1 depicts the conceptual diagram of the FAWT.

As for constructing a wind farm, the wake behind the turbines is important. Researchers have also concentrated on and studied it experimentally and numerically for HAWTs [20,21] and for VAWTs [22,23]. However, most of the object rotors are upright, and there have been few studies on the wake behind tilted rotors. In a study by Guo et al. [24], the center shaft of the rotor was in an upright condition, and only the blades were inclined by using linkage systems. Meanwhile, in the case of FAWTs, the blades and the center shaft of the rotor incline with the spar.

The performance of the FAWT under the tilted conditions was first discussed by the lifting line theory simulation. Then, its wake field was discussed. The simulation results show that a tilted VAWT recovers faster than both a HAWT and an upright VAWT. This indicates that FAWTs can be deployed in high density at an offshore wind farm.

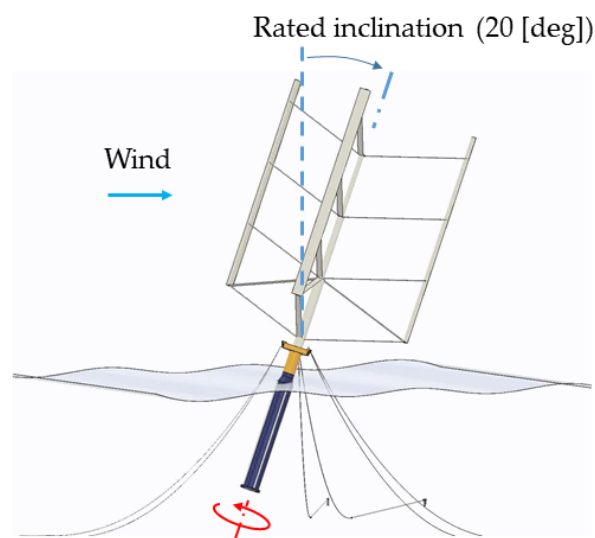


**Figure 1.** Conceptual diagram of Floating Axis Wind Turbine.

## 2. Simulation Methods and Turbine Models

In this study, QBlade with v0.963 was used for estimating the performance and wakes of VAWTs under various conditions. It is an open-source wind turbine calculation software that includes 2-dimensional airfoil calculation and the lifting line free-vortex wake (LLFVW) theory simulation which belongs to the vortex method [25]. By using the vortex method, the flow field is modeled as inviscid, incompressible, and irrotational. The effect of fluid viscosity is modeled by the vortices introduced into the flow field from turbine blades, in this case. The rotor is represented by a lifting line which is located at the quarter chord position of the airfoil cross section. The blades are modeled as a lattice of horseshoe vortices using the vortex lattice method. Figure 2 depicts the modeling used in the LLFVW algorithm.

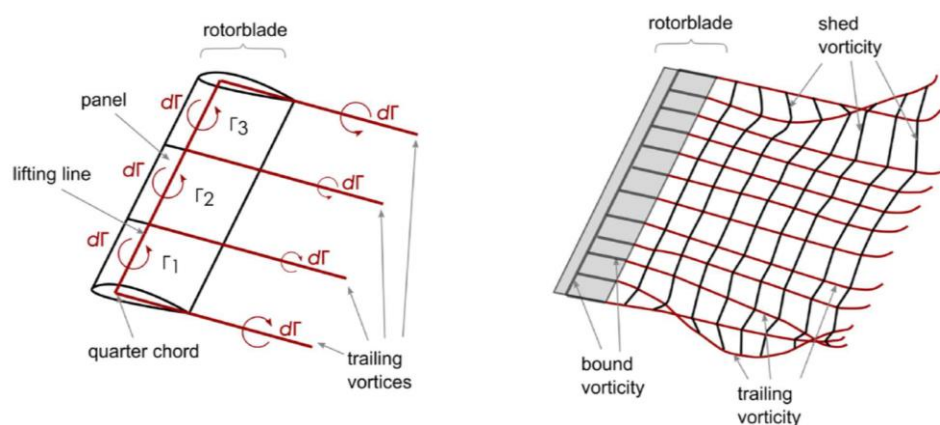


**Figure 2.** Illustration of blade and wake modeling with the LLFVW algorithm [25].

The circulation of the bound vorticity, which forms the lifting line ( $d\Gamma$ ), is calculated based on the Kutta–Joukowski theorem as follows.

$$dL = \rho V_{rel} d\Gamma \quad (1)$$

$dL$  is the sectional lift force and  $V_{rel}$  is the relative velocity. The relative velocity at an arbitrary position in the analysis field is composed of the free-stream velocity, the velocity of blade motion, and the induced velocity from all vortex elements on the blade and in

the wake. The induced velocity from vortex line elements is known as the Biot–Savart law below,

$$V_{ind} = -\frac{1}{4\pi} \int \Gamma \frac{\mathbf{r} \times d\mathbf{l}}{|\mathbf{r}|^3} \quad (2)$$

Meanwhile, the sectional lift force  $dL$  can be calculated from the relative velocity and lift coefficient as follows:

$$dL = \frac{1}{2} \rho V_{rel}^2 dA C_L \quad (3)$$

Then,  $d\Gamma$  is obtained from Equations (1) and (3) with iteration steps. More details, such as the iteration steps and the convection of vortex elements, can be found in the references [26] and [27].

The authors of [28] compared power coefficients obtained by using QBlade and experimental results, such as SANDIA 34-m “Test Bed” Darrieus VAWT [3] and 1 KW DeepWind turbine test model [29], and validated simulation conditions to obtain sufficient results. Based on it, the simulation conditions in this research were determined. In QBlade, users should design the airfoil first and then simulate its polars, such as lift and drag coefficient, within an adequate attack angle ( $\alpha$ ) range by using XFOIL, which is integrated into QBlade. The simulated polars can be extrapolated by using the Viterna or Montgomery method. Then, the rotor is designed with the airfoils. The blade forces are calculated by using the lifting line theory. The circulation of the blade is placed at the 1/4 chord positions and its strength is calculated from airfoil data and  $\alpha$ , which is calculated from the induced velocity of free wake. The wake is represented by the freely floating vortices which are shed from the trailing edge of the blades during every simulation time step. As the simulation time increases, the total number of vortices shed into the flow field also increase and it results in time-consuming calculation of the induced velocity from the vortices. The wake count can be set as rotor revolutions, time steps, or time. The effect from wake in 8 rotor revolutions was considered in this study.

This study employed two turbine models. One has three straight-blade VAWTs. This model was employed to validate the simulation conditions prior to verifying the tilt effect on the performance of VAWTs. Table 1 summarizes its main features. Despite the fact that NACA0018 was used for the blade profile, the lift ( $C_L$ ) and drag coefficient ( $C_D$ ) were defined as the equations that were used in the simulation by Tavernier et al. [30], defined below. Thus, two extrapolated methods described above were not used in this study.

$$C_L = 2\pi \cdot 1.1 \cdot \sin \alpha \quad (4)$$

$$C_D = 0 \quad (5)$$

**Table 1.** Principal particulars of Model 1 (two straight-blade turbines).

Property	Value
Solidity	0.085
Tip Speed Ratio	3
Radius of Rotor [m]	2.5
Aspect Ratio	0.5, 1, 2, 5
Number of Blades	3
Blade Profile	NACA0018

The other model is a VAWT for testing the tilt effect on its performance and discussing the wake field. The constant tilt of the rotor is assumed to be approximately 20 [deg]. Thus, the angle varied from 0 to 40 by 5 degrees. The  $C_L$  and  $C_D$  were calculated by using XFOIL and extrapolated into 360 [deg] using Montgomerie’s method in the 360 Polar Extrapolation Module. Table 2 summarizes the main characteristics of this mode. The corresponding Reynolds number based on the blade chord length and tip speed is approximately from

$1.8 \times 10^4$  to  $3.4 \times 10^4$  for both Model 1 and 2. Flow around the turbine is turbulent under such Reynolds number regions.

**Table 2.** Principal particulars of Model 2 (VAWT under tilted conditions).

Property	Value
Tilt angle of rotor [deg]	0:5:40
Solidity	0.085
Tip Speed Ratio	3
Radius of Rotor [m]	2.5
Aspect Ratio	1, 2
Number of Blades	3
Blade Profile	NACA0018

In QBlade, the viscous effect is tuned by using the parameter “initial core size”. 1/8 of the blade chord length was used in the simulation for both models. This core size is also used in the simulation of CACTUS.

### 3. Results

#### 3.1. Validation of Simulation Conditions

The power ( $C_P$ ) and thrust ( $C_T$ ) coefficients of Model 1, which are defined as the following equations, were compared with Tavernier’s work.

$$C_P = \frac{\text{Power}}{\frac{1}{2}\rho V_\infty^3 2RH} \quad (6)$$

$$C_T = \frac{\text{Thrust}}{\frac{1}{2}\rho V_\infty^2 2RH} \quad (7)$$

They compared the results from several simulation methods, including the 2D actuator cylinder model (AC2D) [31], the 2D actuator cylinder with near-wake correction (HAWC2-NW) [32], CACTUS, free- or fixed-wake vortex model [33], and the Actuator Line OpenFOAM model (TurbinesFoam, end effects) [34]. In CACTUS, “fixed-wake” means that the wake convection velocity is kept constant in time, whereas “free-wake” means that the velocity is calculated at each time step based on the induced velocity. Table 3 depicts the comparisons of such simulation results with those of this study. The aspect ratio of the rotor was 1.0 for these calculations. Compared to other calculation methods, appropriate values were estimated by QBlade.

**Table 3.** Comparisons of Power and Thrust Coefficients.

Method	Power Coefficient ( $C_P$ )	Thrust Coefficient ( $C_T$ )
AC2D	0.510	0.653
HAWC2-NW	0.400	0.570
CACTUS, fixed-wake	0.509	0.647
CACTUS, free-wake	0.486	0.643
TurbineFoam	0.522	0.660
TurbineFoam, end effects	0.469	0.578
QBlade (this study)	0.503	0.665

Figure 3 depicts the comparison of the tangential force acting on a blade in relation to the azimuth angle. Because its  $C_P$  and  $C_T$  were closest to those of this study, the result of CACTUS with fixed wake was cited from reference [26]. In Figure 3, “HD” denotes the rotor’s aspect ratio and the wind comes from 90 [deg]. Thus, azimuth angles of 0~180 and 180~360 [deg] indicate the upwind and leeward side of the blade, respectively. The same trend with respect to the aspect ratio can be seen in both figures. The blade mainly obtains

the energy from wind at around 90 [deg] and also at around 270 [deg]. The results of this study, however, were not smooth on the leeward side. This implies that the initial core size should be adjusted in each case, despite the fact that they were fixed as 8/chord for all aspect ratio cases in this study for comparison.

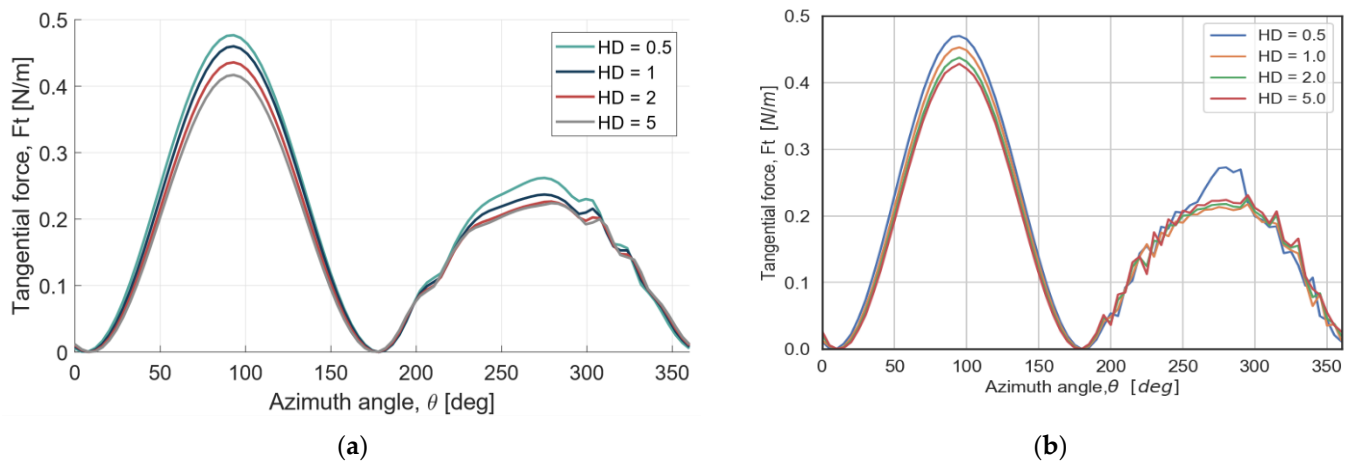


**Figure 3.** Tangential blade force with respect to the azimuth angle (a) CACTUS, fixed-wake [26]; (b) this study (QBlade).

Figure 4 depicts tangential blade forces as a contour graph with respect to the azimuth angle and blade height. This turbine is a 1.0. It is the same as Figure 3 in the sense that azimuth angles 0~180 and 180~360 [deg] indicate upwind and leeward sides of the blade's position, respectively, and wind comes from 90 [deg]. The tangential force is symmetric in a blade spanwise direction, and the ground effect is not taken into account in these simulations. There is no discernible difference between Figure 4a,b.

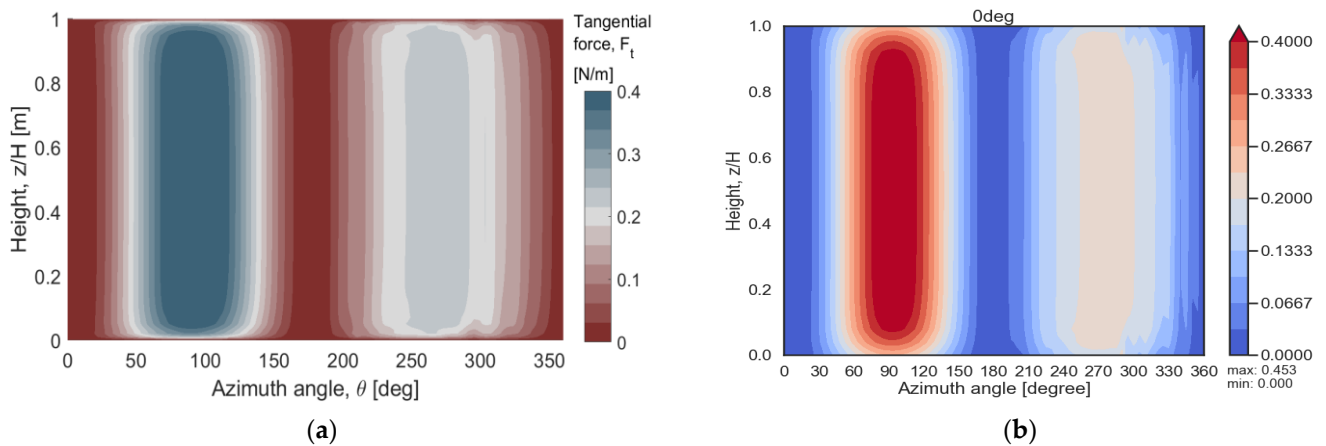


**Figure 4.** Contour graph of tangential blade force: (a) CACTUS, fixed-wake [30]; (b) this study (QBlade).

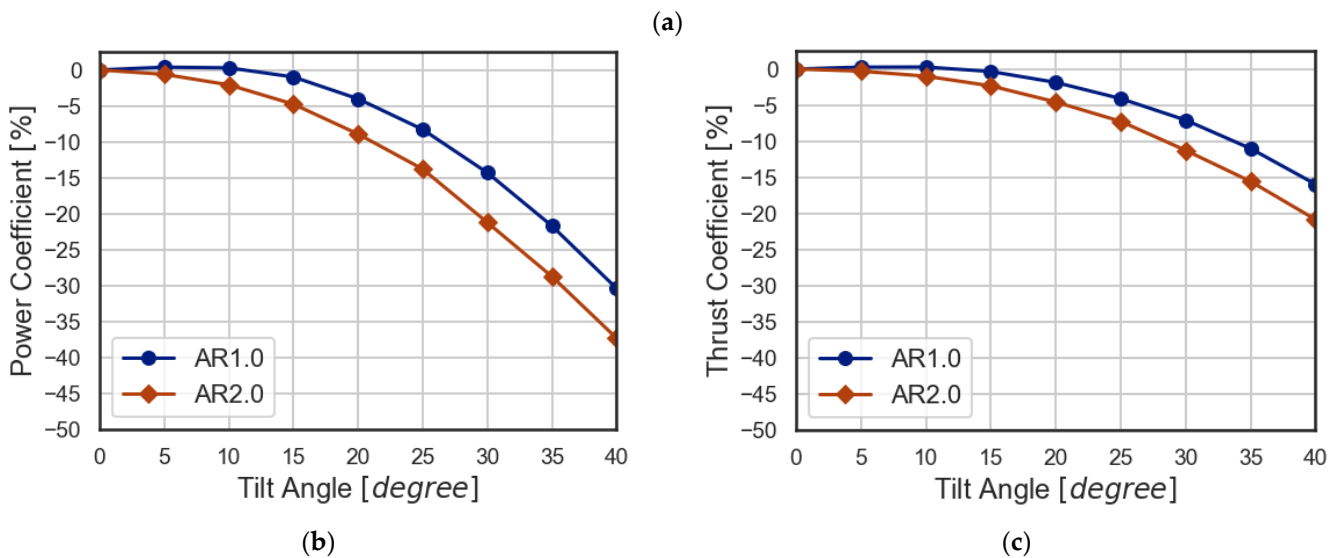
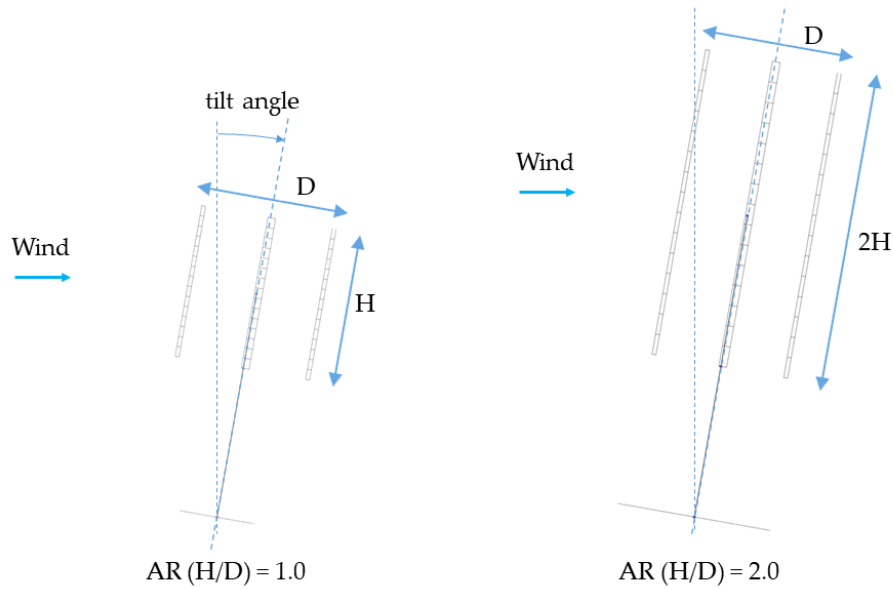
These results demonstrate that the simulation conditions used in this study are appropriate and that such conditions will be used in the following simulations.

### 3.2. Tilt Effect on the Performance of VAWT

#### 3.2.1. Power and Thrust Coefficient of Tilted VAWT

A FAWT is built with the assumption that its rotor will be at a 20-degree tilt under-rated operation;  $C_P$  and  $C_T$  for Model 2 were estimated to assess the tilt effect on VAWT performance. The values are shown in Table 4, and Figure 5 depicts the differences in the

upright condition. These results show that the power coefficient slightly increases at a 10-degree tilt for a rotor with a 1.0 aspect ratio. The decrease in  $C_p$  at a 20-degree tilt is only 4% from the upright condition. This is because the swept area of the VAWT increases when the rotor tilts to some extent [35]. Concerning the rotor with 2.0 aspect ratio, the decrease in performance at a 20-degree tilt is 10% from the upright condition. The decrease in performance for the 2.0 aspect ratio is larger than that for the 1.0 aspect ratio. This is explained by the fact that the rotor radius contributes to the increase in swept area, which becomes relatively small as the aspect ratio increases.

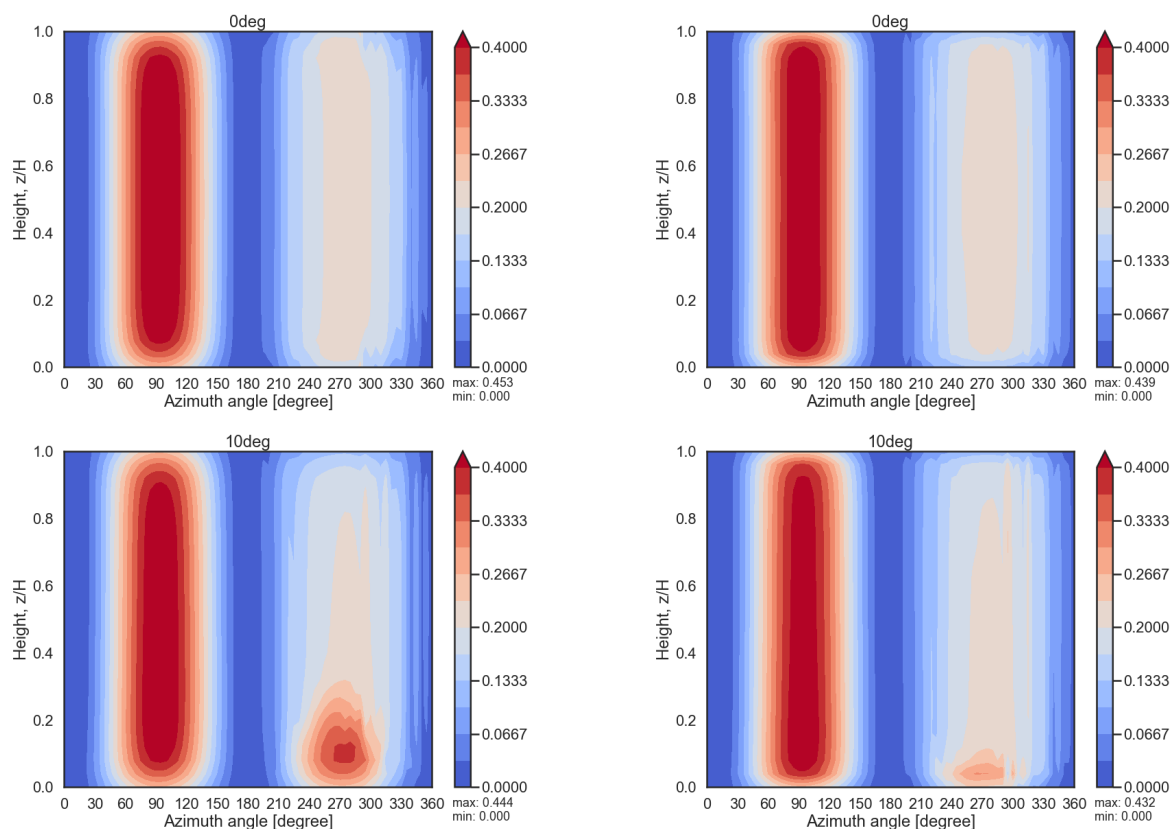


**Figure 5.** Difference in Power and Thrust Coefficients of a tilted rotor compared to an upright one: (a) configuration of the simulation; (b) power coefficient; (c) thrust coefficient.

**Table 4.** Power and Thrust coefficients with respect to tilted angle.

Aspect Ratio	1.0		2.0	
Tilt Angle [deg]	$C_P$	$C_T$	$C_P$	$C_T$
0	0.503	0.665	0.500	0.662
5	0.504	0.667	0.497	0.660
10	0.505	0.667	0.489	0.655
15	0.498	0.662	0.476	0.647
20	0.483	0.652	0.455	0.632
25	0.462	0.638	0.431	0.614
30	0.431	0.618	0.394	0.588
35	0.394	0.592	0.356	0.559
40	0.350	0.559	0.313	0.524

Figure 6 depicts the tangential blade forces as a contour graph in relation to the azimuth angle and blade height. Because the blade height is normalized, the height effect appears in a 2.0 aspect ratio. These figures depict that in the case of a tilted rotor, the lower part of the rotor on the leeward side effectively obtains energy from wind. Under the upright condition, wind velocity on the leeward side decreases from the top to the bottom of the blade height. Meanwhile, when the rotor is in the tilted condition, the wind velocity on the lower part of the rotor on the leeward side stays strong because the blade does not pass the wind on the upwind side. Then, the lower part of the rotor obtains energy from the wind on the leeward side. Even though the smallest part of the rotor can effectively generate the tangential force on the leeward side, the airfoil performance degrades with increasing rotor tilt angle. This may be indicated in the results of the 30- and 40-degree-tilt tests. Based on these findings, it stands to reason that the FAWT rotor is at a 20-degree tilt under the rated operation.

**Figure 6.** Cont.

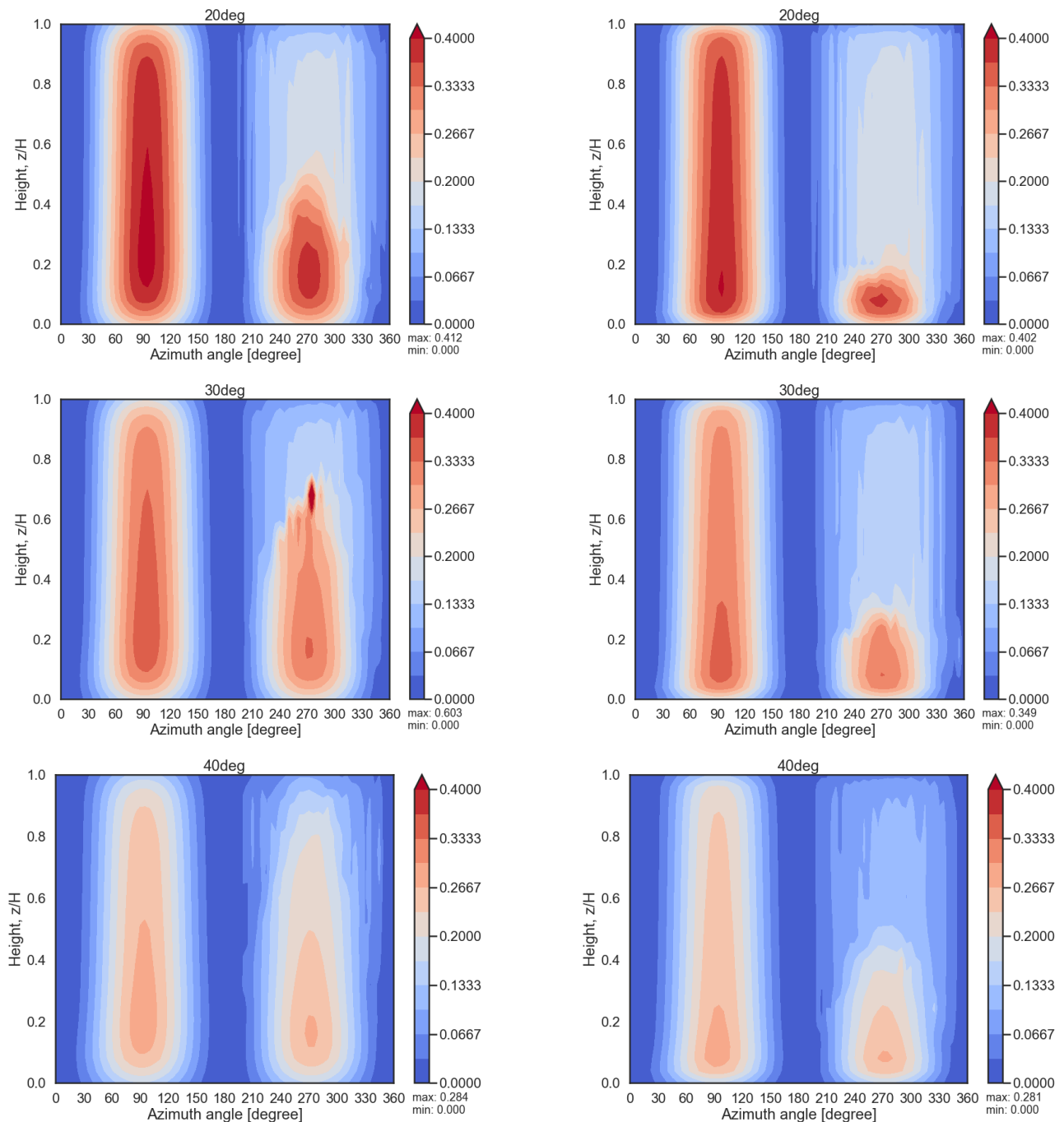
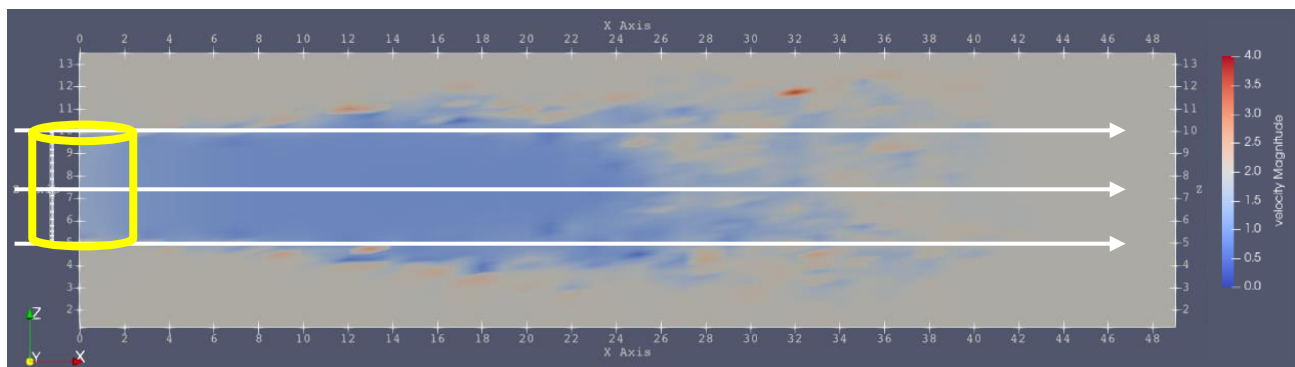


**Figure 6.** Contour graph of tangential blade force for 0-, 10-, 20-, 30-, and 40-degree-tilted rotors.

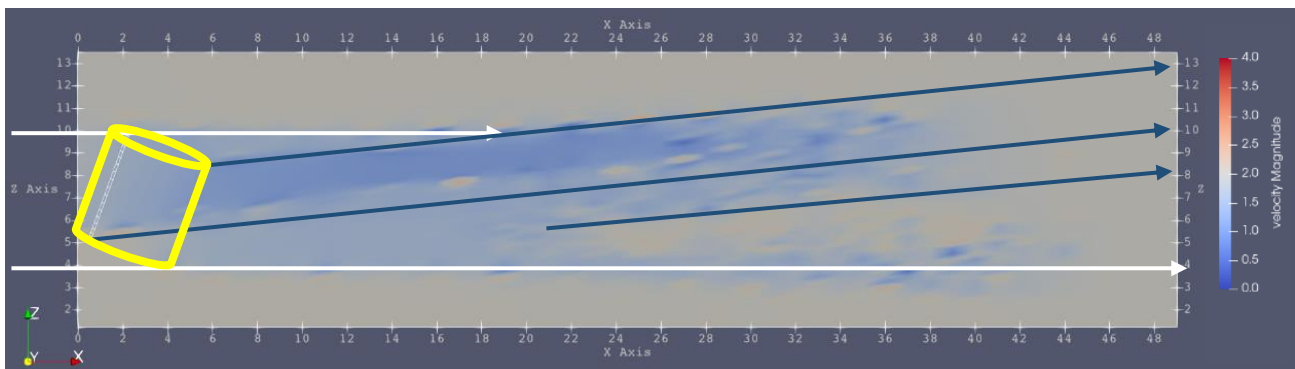
### 3.2.2. The Wake Field of the Tilted VAWT

The installation interval of wind turbines is an important factor to consider when building a wind farm. As a result, the wake field of a VAWT was assessed. The target VAWT is Model 2 with a 1.0 aspect ratio. Figure 7 depicts the instantaneous velocity field center section (XZ-plane) of an upright, 20-degree-tilted VAWT and an upright HAWT. The X-axis is in the direction of the wind, and the coordinate system (O-XYZ) is right-handed. The rotor is represented by a yellow circular cylinder, and the contour color indicates the magnitude of in-plane wind velocity nondimensionalized by uniform flow. The result for the HAWT was simulated by using a sample project of a HAWT contained in QBlade by default. In the case of the upright VAWT and HAWT, the wake goes straight to the leeward

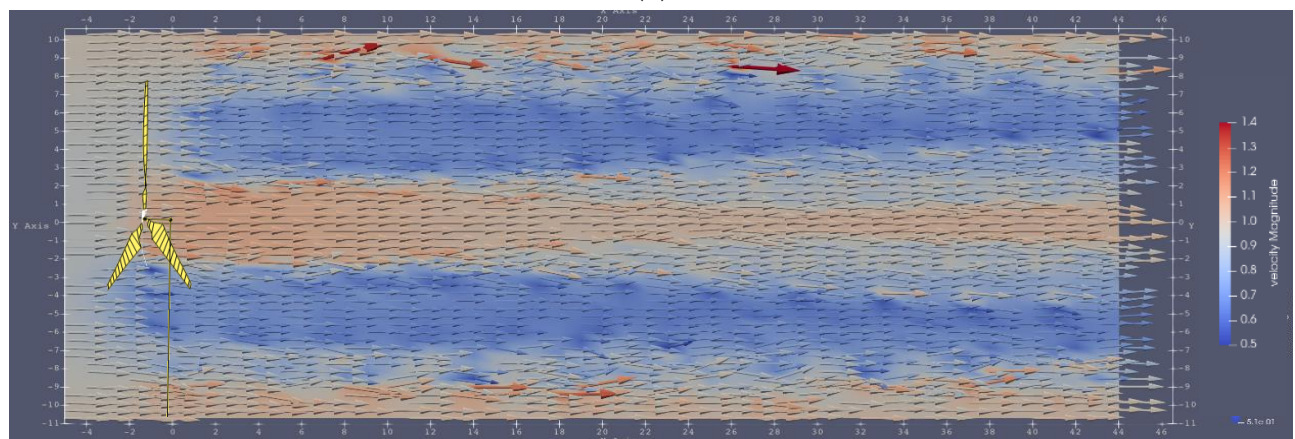
side. Meanwhile, in the case of a 20-degree-tilted VAWT, the wake goes upward. The inclination angle is approximately 6 [deg].



(a)



(b)

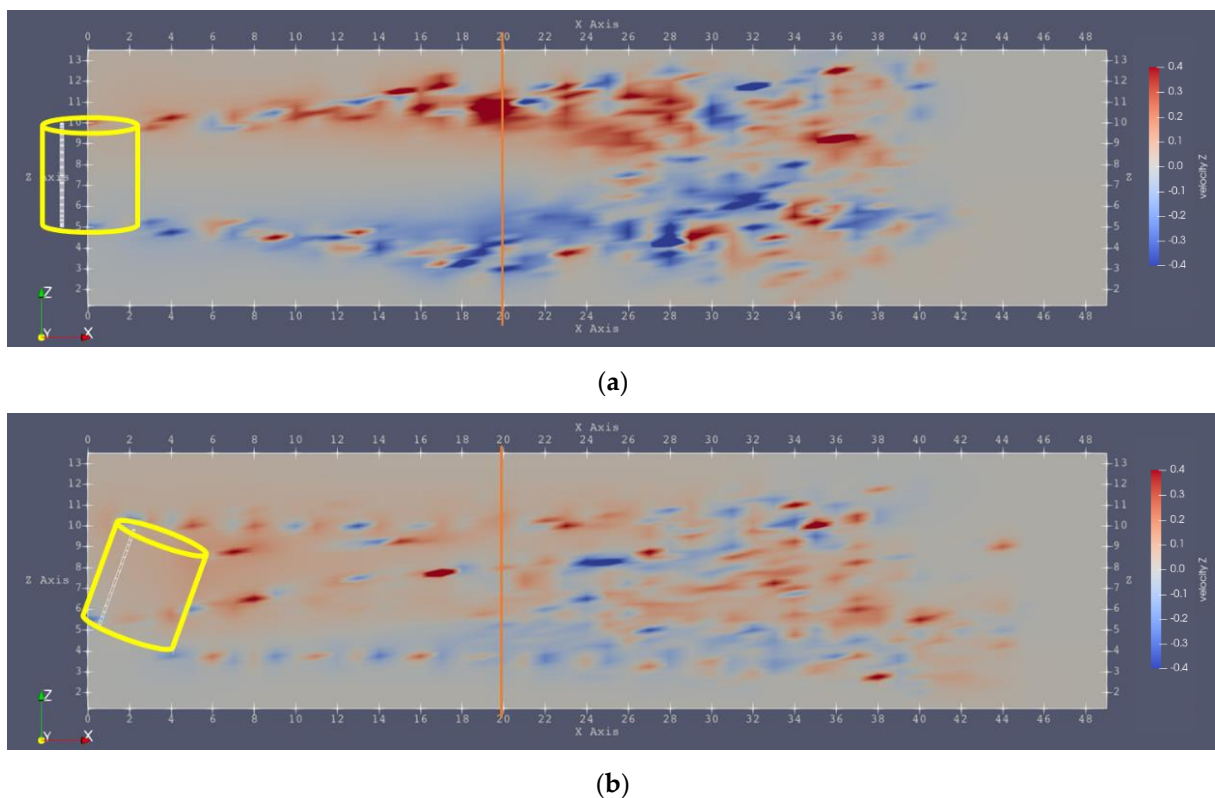


(c)

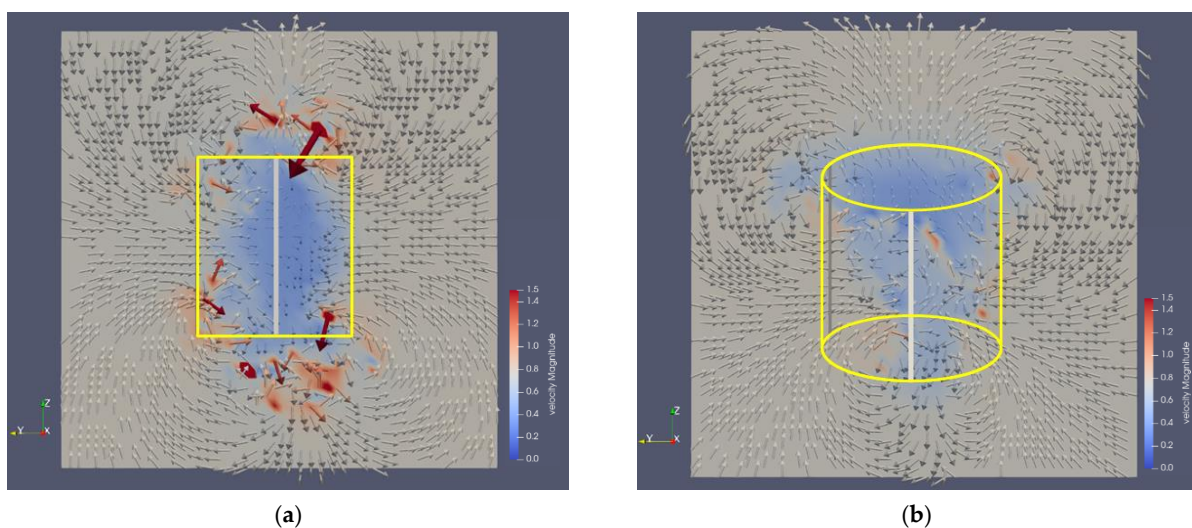
**Figure 7.** Magnitude of in-plane wind velocity: (a) upright VAWT; (b) 20-degree-tilted VAWT; (c) upright HAWT.

Figure 8 depicts the vertical component of wind velocity corresponding to Figure 7. The colors red and blue represent the upward and downward velocity components, respectively. Compared to the flow field of an upright VAWT, the upward velocity component may be seen just behind the rotor, as opposed to the flow field of an upright VAWT. The orange lines denote the position at four times the rotor diameter's ( $D$ ) distance from the rotor center, and Figure 9 depicts the wind velocity vector in the  $YZ$ -plane at that location. The yellow circular cylinder represents the rotor's position, which is located  $4D$  anteriorly. The color of the contour indicates the magnitude of the velocity in this plane. The colors blue

and red represent low and high velocity, respectively. There are upward and downward vectors at the top and bottom of the rotor in both cases. Then, the vectors head into the center region from both sides of the top of the rotor. Figure 10 depicts 3D streamlines of an upright and 20-degree-tilted VAWT. In these figures, the blades of the rotor are shown in black. Under the upright condition, most of the streamlines behind the turbine go straight to the leeward side. On the other hand, the streamlines go obliquely upward under the 20-degree-tilted condition. These results indicate that the momentum is being transferred between the lower- and the higher-velocity region. As a result, the wind velocity at rotor height recovers to its initial velocity faster than that of a HAWT. This allows us to install VAWTs in a dense manner.



**Figure 8.** Contour of the vertical component of wind velocity: (a) upright; (b) 20-degree tilt.



**Figure 9.** Wind velocity vector in the YZ-plane (a) upright; (b) 20-degree tilt.

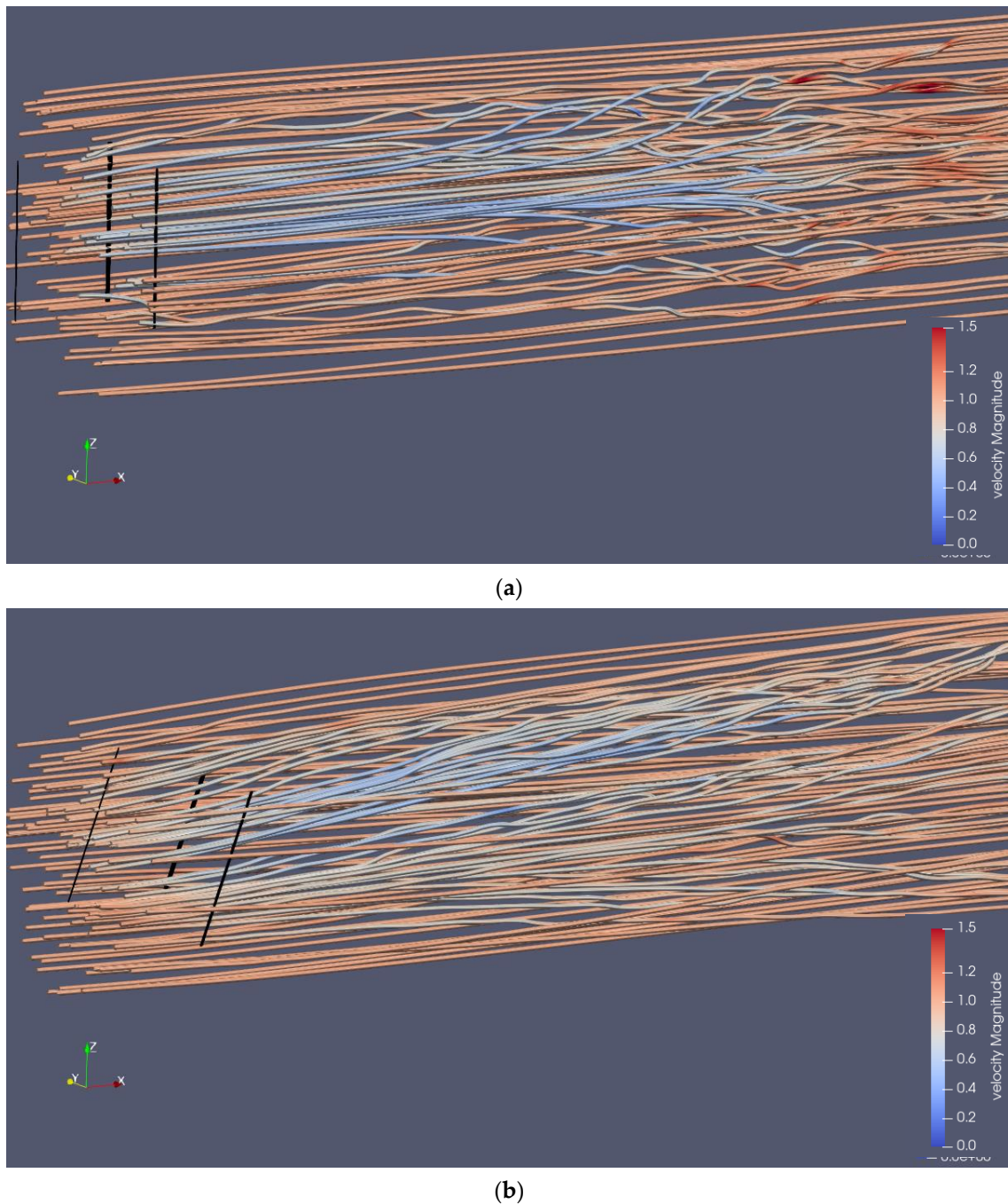
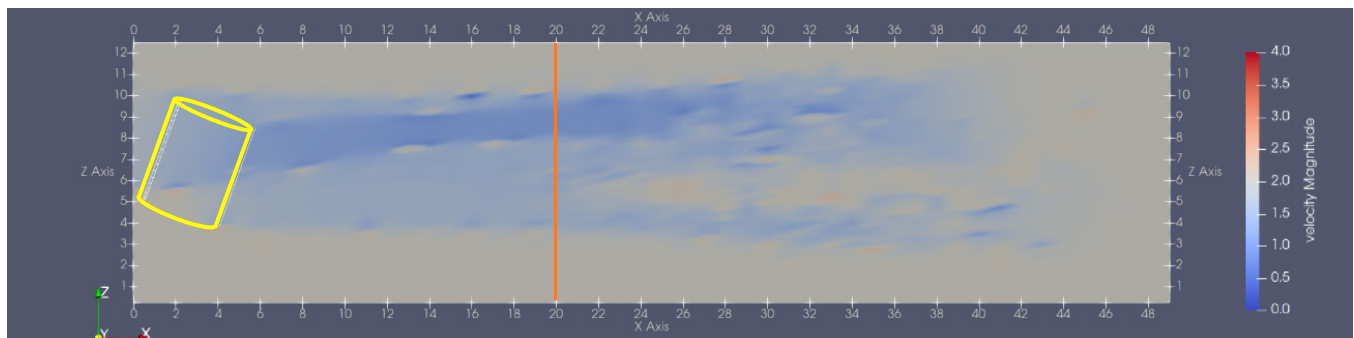


**Figure 10.** 3D Streamlines (a) upright; (b) 20-degree tilt.

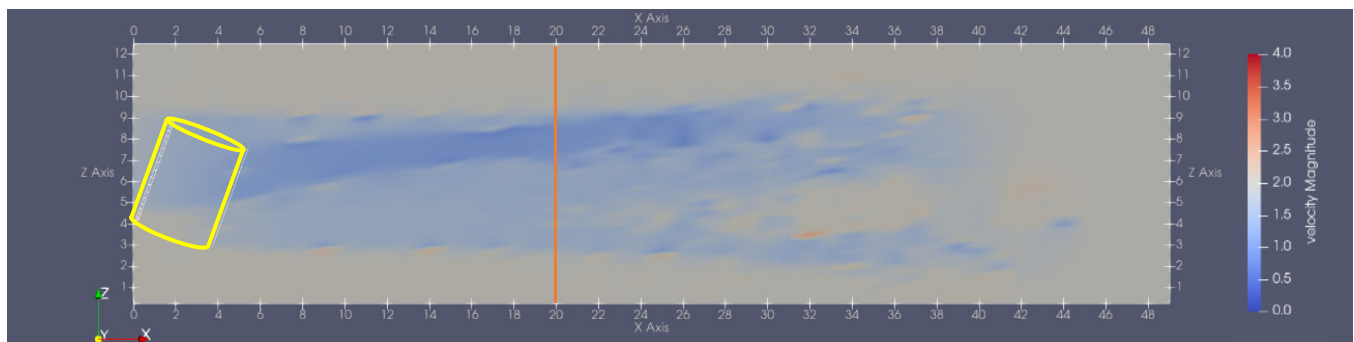
### 3.2.3. Ground Effect

The ground effect was not considered in the previous section's simulations, so as to verify only the tilt effect on its wake field. Even if the FAWT is properly designed so that the blades do not hit the sea surface when the rotor inclines, the clearance between the rotor blade bottom and the sea surface will affect the wake field when the tilted condition occurs. QBlade implements the ground effect by mirroring the rotor blade and wake vortices at the ground plane. The clearance has been changed from 1.0D, 0.8D, 0.6D, and 0.4D. For all cases, the rotor tilt angle was kept constant at 20 [deg]. The instantaneous velocity field at the center section (XZ-plane) of a 20-degree-tilted VAWT with various ground clearances is depicted in Figure 11. The orange lines represent the position at 4D from the rotor center, and Figure 12 depicts the wind velocity vector in the YZ-plane at that location. In all cases,

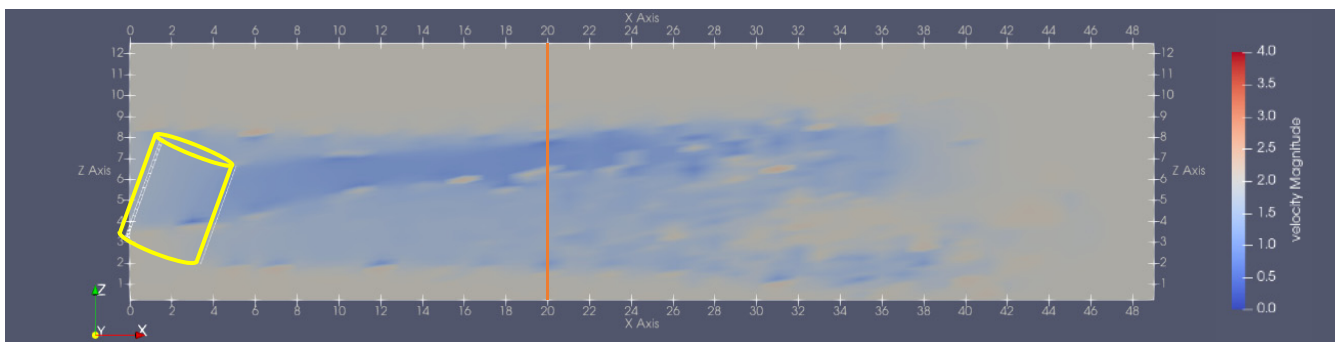
the upward wind may be seen behind the VAWT, but the smaller the clearance becomes, the greater the distance that velocity recovers.



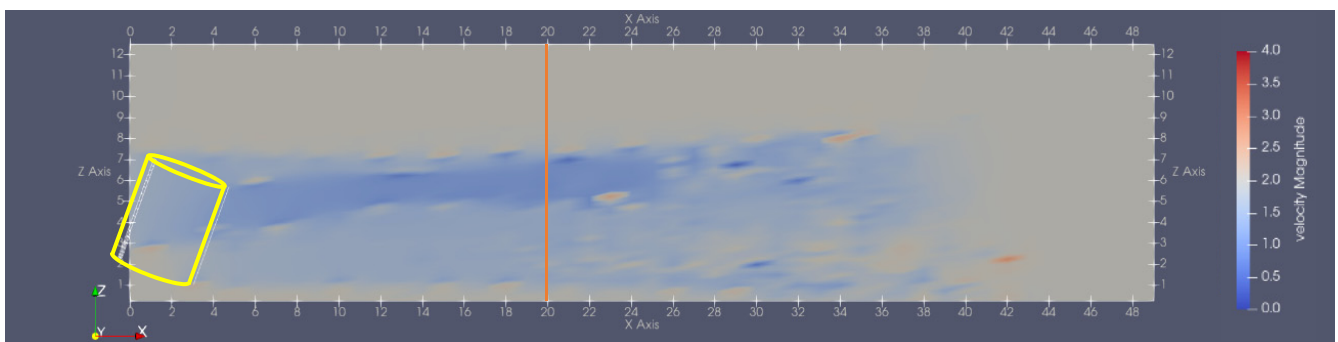
(a)



(b)



(c)



(d)

**Figure 11.** Magnitude of in-plane wind velocity behind a 20-degree-tilted VAWT with different ground clearance: (a) 1.0D; (b) 0.8D; (c) 0.6D; (d) 0.4D.

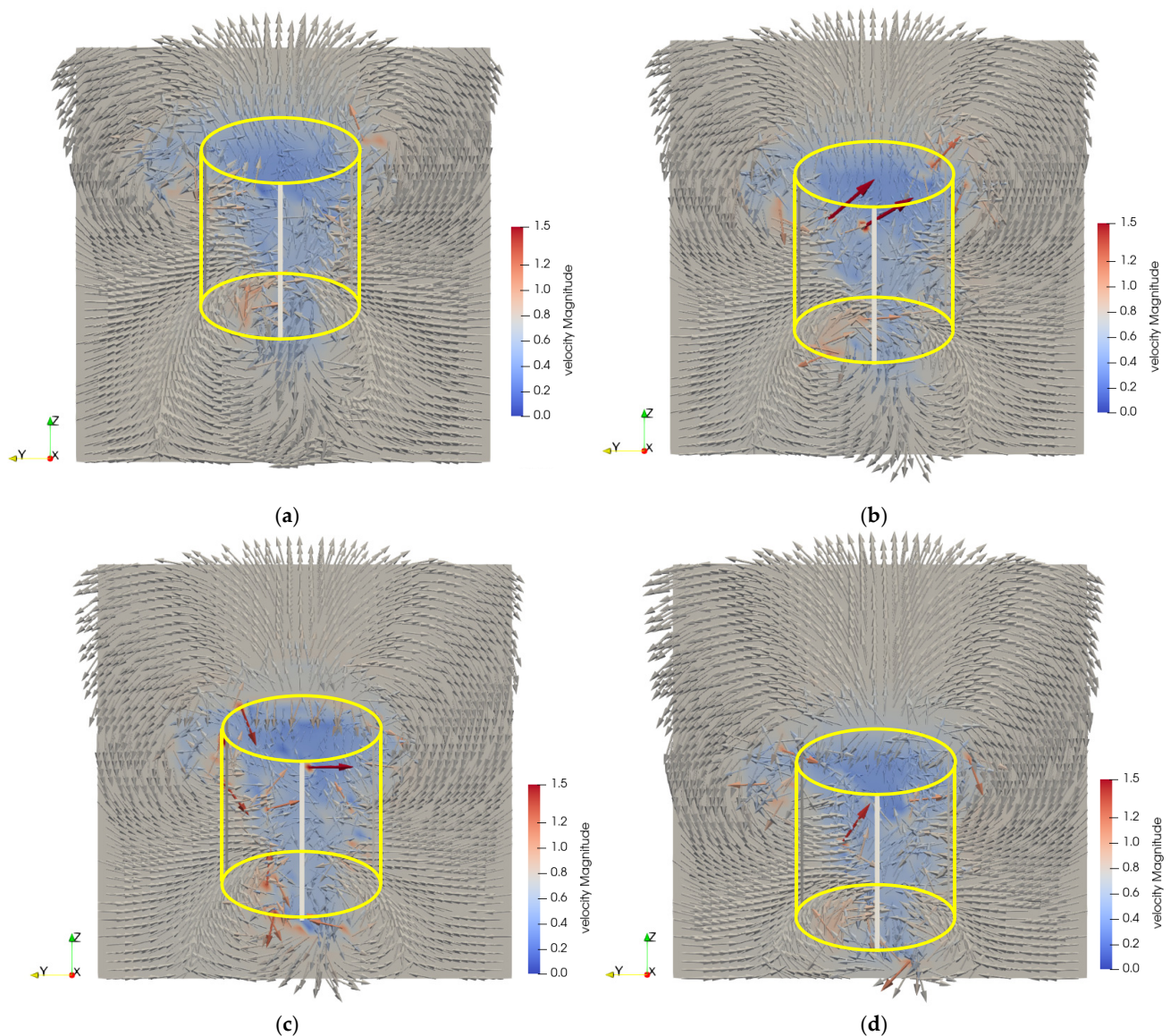


**Figure 12.** Wind velocity vector in the YZ-plane behind a 20-degree-tilted VAWT with different ground clearance: (a) 1.0D; (b) 0.8D; (c) 0.6D; (d) 0.4D.

#### 4. Conclusions

The performance and wakes of VAWTs were simulated in this study using liftingline theory simulation. The simulation conditions were validated using a VAWT model with three straight blades. When compared to the results of the other simulation methods, the simulation conditions used in this study were found to be appropriate. Then, the tilt effect on the performance and wake field of VAWTs were evaluated with the other VAWT model, and the following results were obtained:

At a 10-degree tilt, the power coefficient of a 1.0 aspect-ratio rotor increases slightly. Then, at a 20-degree tilt, the decrease in  $C_p$  is only 4% from the upright condition. This increase in the power coefficient with respect to the tilt is in agreement with Balduzzi's work [35], and it is explained by the contour graph of the tangential force on the blade, which shows that in the case of a tilted rotor, the lower part of the rotor at the leeward side effectively obtains the energy from wind. Meanwhile, as the rotor tilt angle increases, so does the performance of the airfoil. Because the increased swept area becomes relatively small as the aspect ratio increases, the performance for the 2.0 aspect ratio decreases more than that for the 1.0 aspect ratio. This, as a result, it is important for VAWTs that the

relationship between the increase in swept area and the decrease in airfoil performance be maintained.

The VAWT wake field was then simulated in order to evaluate the installation interval of wind turbines. The upward velocity component appears just behind the rotor, and the wake goes obliquely upward approximately 6 [deg] from the horizontal plane, whereas the wake for the upright VAWT and HAWT goes straight to the leeward side. The velocity field of the plane perpendicular to the wind direction indicates that there are upward and downward velocity components at the top of the rotor's height and the bottom side of the VAWT, respectively. Furthermore, the velocity components at the top of the rotor head into the center region from both sides of the rotor. They result in a momentum exchange. The wind velocity at the top of the rotor of a tilted VAWT recovers to its initial velocity faster than that of a HAWT, allowing us to install VAWTs more densely.

Even though the ground effect was taken into account, the wake goes upward for tilted VAWTs. However, the smaller the clearance between the sea surface and the blades of a tilted VAWT becomes, the further the distance that velocity recovers.

**Author Contributions:** Conceptualization, H.S., H.U. and H.A.; methodology, H.S., H.U. and H.A.; data curation, H.S. and H.U.; writing—original draft preparation, H.S.; writing—review and editing, H.S.; project administration, H.A. All authors have read and agreed to the published version of the manuscript.

**Funding:** This research received no external funding.

**Data Availability Statement:** Not applicable.

**Conflicts of Interest:** The authors declare no conflict of interest.

## Nomenclature

$C_p$	power coefficient
$C_L$	lift coefficient
$C_D$	drag coefficient
$C_T$	thrust coefficient
$D$	rotor diameter [m]
$dA$	cross-sectional area [m <sup>2</sup> ]
$dL$	sectional lift force [N]
$dl$	line element vector [m]
$d\Gamma$	sectional circulation [m <sup>2</sup> /s]
$H$	rotor height [m]
$\rho$	air density [kg/m <sup>3</sup> ]
$R$	rotor radius [m]
$\mathbf{r}$	relative position vector [m]
$V_{ind}$	induced velocity from vortex line element [m/s]
$V_{rel}$	relative velocity [m/s]
$V_\infty$	free-stream velocity [m/s]
$\alpha$	attack angle [deg]

## References

1. International Energy Agency. Offshore Wind Outlook. 2019. Available online: <https://www.iea.org/reports/offshore-wind-outlook-2019> (accessed on 8 April 2022).
2. Global Wind Energy Council. Global Offshore Wind Report. 2021. Available online: <https://gwec.net/global-offshore-wind-report-2021/> (accessed on 8 April 2022).
3. Pope, K.; Dincer, I.; Naterer, G.F. Energy and exergy efficiency comparison of horizontal and vertical axis wind turbines. *Renew. Energy* **2010**, *35*, 2102–2113. [CrossRef]
4. Mendoza, V.; Chaudhari, A.; Goude, A. Performance and wake comparison of horizontal and vertical axis wind turbines under varying surface roughness conditions. *Wind. Energy* **2019**, *22*, 458–472. [CrossRef]

5. Johnston, S.F., Jr. *Proceedings of the Vertical Axis Wind Turbine (VAWT) Design Technology Seminar for Industry*; SANDIA REPORT, SAND80-0984; Sandia National Laboratories: Albuquerque, NM, USA, 1982.
6. Sutherland, H.J.; Berg, D.E.; Ashwill, T.D. *A Retrospective of VAWT Technology*; SANDIA REPORT, SAND2012-0304; Sandia National Laboratories: Albuquerque, NM, USA, 2012.
7. Daegyoun, K.; Morteza, G. Efficiency improvement of straight-bladed vertical-axis wind turbines with an upstream deflector. *J. Wind Eng. Ind. Aerodyn.* **2013**, *115*, 48–52. [[CrossRef](#)]
8. Watanabe, K.; Takahashi, S.; Ohya, Y. Application of a diffuser structure to vertical-axis wind turbines. *Energies* **2016**, *9*, 406. [[CrossRef](#)]
9. Hou, L.; Shen, S.; Wang, Y. Numerical study on aerodynamic performance of different forms of adaptive blades for vertical axis wind turbines. *Energies* **2021**, *14*, 880. [[CrossRef](#)]
10. Hara, Y.; Horita, N.; Yoshida, S.; Akimoto, H.; Sumi, T. Numerical analysis of effects of arms with different cross-sections on straight-bladed vertical axis wind turbine. *Energies* **2019**, *12*, 2106. [[CrossRef](#)]
11. Aihara, A.; Mendoza, V.; Goude, A.; Bernhoff, H. Comparison of three-dimensional numerical methods for modeling of strut effect on the performance of a vertical axis wind turbine. *Energies* **2022**, *15*, 2361. [[CrossRef](#)]
12. Yang, Y.; Guo, Z.; Song, Q.; Zhang, Y.; Li, Q. Effect of blade pitch angle on the aerodynamic characteristics of a straight-bladed vertical axis wind turbine based on experiments and simulations. *Energies* **2018**, *11*, 1514. [[CrossRef](#)]
13. Horb, S.; Fuchs, S.; Immas, A.; Silvert, F.; Deglaire, P. Variable pitch control for vertical-axis wind turbines. *Wind Eng.* **2018**, *42*, 128–135. [[CrossRef](#)]
14. Mohammed, A.A.; Sahin, A.Z.; Ouakad, H.M. Numerical investigation of a vertical axis wind turbine performance characterization using new variable pitch control scheme. *J. Energy Resour. Technol.* **2020**, *142*, 031302. [[CrossRef](#)]
15. Akimoto, H.; Tanaka, K.; Uzawa, K. Floating axis wind turbines for offshore power generation—a conceptual study. *Environ. Res. Lett.* **2011**, *6*, 044017. [[CrossRef](#)]
16. Blusseau, P.; Patel, M.H. Gyroscopic effects on a large vertical axis wind turbine mounted on a floating structure. *Renew. Energy* **2012**, *46*, 31–42. [[CrossRef](#)]
17. Ishie, J.; Wang, K.; Ong, M.C. Structural dynamic analysis of semi-submersible floating vertical axis wind turbines. *Energies* **2016**, *9*, 1047. [[CrossRef](#)]
18. Paulsen, U.S.; Borg, M.; Madsen, H.A.; Pedersen, T.F.; Hattel, J.; Ritchie, E.; Ferreira, C.S.; Svendsen, H.; Berthelsen, P.A.; Smadja, C. Outcomes of the DeepWind conceptual design. *Energy Procedia* **2015**, *80*, 329–341. [[CrossRef](#)]
19. Wen, T.R.; Wang, K.; Cheng, Z.; Ong, M.C. Spar-type vertical-axis wind turbines in moderate water depth: A feasibility study. *Energies* **2018**, *11*, 555. [[CrossRef](#)]
20. Lignarolo, L.E.M.; Ragni, D.; Krishnaswami, C.; Chen, Q.; Ferreira, C.J.S.; Bussel, G.J.W. Experimental analysis of the wake of a horizontal-axis wind-turbine model. *Renew. Energy* **2014**, *70*, 31–46. [[CrossRef](#)]
21. Rezaeiha, A.; Micallef, D. Wake interactions of two tandem floating offshore wind turbines: CFD analysis using actuator disc model. *Renew. Energy* **2021**, *179*, 859–876. [[CrossRef](#)]
22. Tescione, G.; Ragni, D.; He, C.; Ferreira, C.J.S.; Bussel, G.J.W. Near wake flow analysis of a vertical axis wind turbine by stereoscopic particle image velocimetry. *Renew. Energy* **2014**, *70*, 47–61. [[CrossRef](#)]
23. Yuan, Z.; Jiang, J.; Zang, J.; Sheng, Q.; Sun, K.; Zhang, X.; Ji, R. A fast two-dimensional numerical method for the wake simulation of a vertical axis wind turbine. *Energies* **2021**, *14*, 49. [[CrossRef](#)]
24. Guo, J.; Lei, L. Flow characteristics of a straight-bladed vertical axis wind turbine with inclined pitch axes. *Energies* **2020**, *13*, 6281. [[CrossRef](#)]
25. Marten, D. *QBLADE v0.95 Guidelines for Lifting Line Free Vortex Wake Simulations*; Technical University Berlin: Berlin, Germany, 2016. [[CrossRef](#)]
26. Van Garrel, A. *Development of a Wind Turbine Aerodynamics Simulation Module*; Technical Report ECN-C-03-079; ECN Wind Energy: Petten, The Netherlands, 2003.
27. Marten, D.; Lennie, M.; Pechlivanoglou, G.; Nayeri, C.N.; Paschereit, C.O. Implementation, Optimization, and Validation of a Nonlinear Lifting Line-Free Vortex Wake Module Within the Wind Turbine Simulation Code QBLADE. *J. Eng. Gas Turbines Power* **2016**, *138*, 072601. [[CrossRef](#)]
28. Senga, H.; Akimoto, H.; Fukai, K. Power Coefficient Estimation of Floating Axis Wind Turbine by Lifting Line Theory. *IOP Conf. Ser. Mater. Sci. Eng.* **2021**, *1051*, 012057. [[CrossRef](#)]
29. Battisti, L.; Benini, E.; Brighenti, A.; Castelli, M.R.; Dell’Anna, S.; Dossena, V.; Persico, G.; Paulsen, U.S.; Pedersen, T.F. Wind tunnel testing of the DeepWind demonstrator in design and tilted operating conditions. *Energy* **2016**, *111*, 484–497. [[CrossRef](#)]
30. Tavernier, D.D.; Sakib, M.; Griffith, T.; Pirrung, G.; Paulsen, U.; Madsen, H.; Keijer, W.; Ferreira, C. Comparison of 3D aerodynamic models for vertical-axis wind turbines: H-rotor and  $\Phi$ -rotor. *Int. J. Phys. Conf. Ser.* **2020**, *1618*, 052041. [[CrossRef](#)]
31. Madsen, H.A. On the Ideal and Real Energy Conversion in a Straight Bladed Vertical Axis Wind Turbine. Ph.D. Thesis, Aalborg University, Aalborg, Denmark, 1983.
32. Beddoes, T.S. A near wake dynamic model. In Proceedings of the AHS National Specialist Meeting on Aerodynamics and Aeroacoustics, Arlington, TX, USA, 25–27 February 1987.

33. Murray, J.C.; Barone, M. The development of CACTUS, a wind and marine turbine performance simulation code. In Proceedings of the 49th AIAA Aerospace Sciences Meeting Including the New Horizons Forum and Aerospace Exposition, Orlando, FL, USA, 4–7 January 2011; AIAA 2011–147. AIAA: Reston, VA, USA, 2011.
34. Bachant, P.; Goude, A.; Wosnik, M. Turbines Foam/Turbinesforam: v0.0.8, Zenodo. 2018. Available online: <https://doi.org/10.5281/zenodo.1210366> (accessed on 8 April 2022).
35. Balduzzi, F.; Bianchini, A.; Carnevale, E.A.; Ferrari, L.; Magnani, S. Feasibility analysis of a Darrieus vertical-axis wind turbine installation in the rooftop of a building. *Appl. Energy* **2012**, *97*, 921–929. [[CrossRef](#)]